

HandsFormer: Keypoint Transformer for Monocular 3D Pose Estimation of Hands and Object in Interaction

Shreyas Hampali⁽¹⁾, Sayan Deb Sarkar⁽¹⁾, Mahdi Rad⁽¹⁾, Vincent Lepetit^(2,1)

⁽¹⁾Institute for Computer Graphics and Vision, Graz University of Technology, Graz, Austria

⁽²⁾Université Paris-Est, École des Ponts ParisTech, Paris, France

{<firstname>.<lastname>}@icg.tugraz.at, vincent.lepetit@enpc.fr

Abstract

We propose a robust and accurate method for estimating the 3D poses of two hands in close interaction from a single color image. This is a very challenging problem, as large occlusions and many confusions between the joints may happen. Our method starts by extracting a set of potential 2D locations for the joints of both hands as extrema of a heatmap. We do not require that all locations correctly correspond to a joint, not that all the joints are detected. We use appearance and spatial encodings of these locations as input to a transformer, and leverage the attention mechanisms to sort out the correct configuration of the joints and output the 3D poses of both hands. Our approach thus allies the recognition power of a Transformer to the accuracy of heatmap-based methods. We also show it can be extended to estimate the 3D pose of an object manipulated by one or two hands. We evaluate our approach on the recent and challenging InterHand2.6M and HO-3D datasets. We obtain 17% improvement over the baseline. Moreover, we introduce the first dataset made of action sequences of two hands manipulating an object fully annotated in 3D and will make it publicly available.

1. Introduction

3D hand pose estimation has the potential to make virtual reality, augmented reality, and interaction with computers and robots much more intuitive. Recently, significant progress has been made for single-hand pose estimation using depth maps and even single RGB images. Being able to deal with RGB images is particularly attractive as it does not require a power-hungry active sensor. Many approaches have been proposed: Direct prediction with different convolutional network architectures [19, 60, 14, 30, 44, 49, 37] of the 3D joint locations or angles, and relying on rendering for fine pose estimation and tracking [2, 33, 11, 40, 50].

In contrast to single-hand pose estimation, two-hand

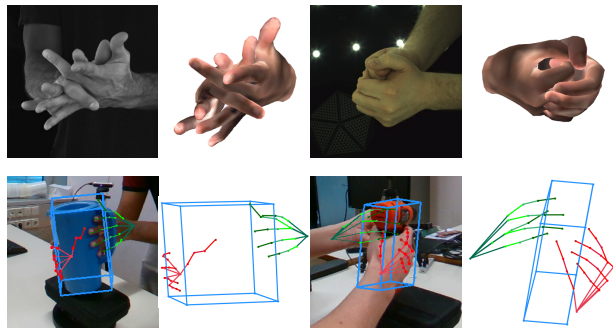


Figure 1: Our architecture enables the estimation of accurate 3D hand and object poses from a single RGB image in a wide range of scenarios. We recover 3D poses during complex hand interactions (top row) and during hands-object interaction where the hand is severely occluded (bottom row)

pose estimation has received much less attention. This problem is indeed significantly harder: The appearance similarities between the joints of the two hands make their identification extremely challenging. Moreover, in close interaction, some of the joints of a hand are likely to be occluded by the other hand or the same hand. Thus, first detecting the left and right hands before independently predicting their 3D poses [12, 37] performs poorly in close interaction scenarios. Bottom-up approaches that first estimate the 2D joint locations and their depths [31, 54] will struggle to deal with the joint similarities and occlusions when trying to identify them.

As shown in Fig. 1, in this work, we identify the joints of *both* hands and predict their 3D locations or angles *jointly* using a transformer [53] from a single color image. We first localize the potential joints in 2D as keypoints from a predicted heatmap, as localizing the joints in 2D is proven to be more accurate than directly regressing their 3D locations [19]. At this stage, the keypoints are not associated with specific joints yet, some keypoints may not correspond to joints at all, and some joints may not be detected as keypoints. The keypoints, however, are a very good starting

point to predict an accurate 3D pose for both hands.

From the keypoints, we predict the pose of both the hands using a transformer encoder-decoder architecture trained end-to-end along with the keypoint detector. Thanks to self-attention mechanisms of the transformer, our architecture collaboratively reasons about the hand joint locations in the input image, leading to more reliable pose estimates than other existing approaches especially during close interactions. The transformer architecture also accepts varying input sizes, which lets us adapt easily to the number of extracted keypoints, which can vary between two different input images. These two properties, self-attention and varying number of inputs, make the transformer architecture a very attractive choice for this task. Moreover, we show that our approach extends naturally to also estimate the 3D pose of an object manipulated by the hands, by sampling keypoints on the object.

Transformers have already been used recently for 3D pose estimation in a few works, but in a different manner. [28] regresses the mesh vertices of a human body or a hand from a single RGB image using multiple layers of transformer encoder. [17] estimates the hand pose from point cloud data using encoder-decoder transformer architecture. While these works are aimed at single hand pose estimation and their extension to two hands is non-trivial, our architecture is designed to estimate single and two-hands poses along with the object pose during hand-object interaction from the input RGB image.

In Computer Vision problems [22, 8, 59, 9, 28, 17, 57, 25], transformers primarily model relationships between features at every image location, thereby drastically increasing the computational complexity as the resolution of the feature map increases [59], especially compared to more standard CNNs. Because of this, transformers typically work on lower resolution feature maps which do not capture finer image details, such as closely spaced hand joints in our case. As we show in our experiments, lower resolution feature maps are not sufficient to estimate hand poses accurately. [59] partially addresses this concern by allowing features at every spatial location to attend to a small set of features from sampled locations across different scales, resulting in more accurate detection of small objects in the image.

In this work, we take one more step in this direction by modelling relationships between only sampled features from high and low resolution feature maps, where the sampling locations are the keypoints provided by a CNN which has been proven effective in detecting finer image details [42]. For the task of pose estimation, we show that such sparsely sampled features are effective in accurately estimating the 3D poses of hands and object when they are closely interacting with each other.

We train and evaluate our architecture on the recent In-

terHand2.6M hand-hand [31] and HO-3D hand-object [11] interaction datasets. We also introduce the first dataset of videos with two hands interacting with an object with complete and accurate 3D annotations without markers. This dataset is based on the work of [11], and we call it H₂O-3D. Our method achieves state-of-the-art performance on existing hand-interaction datasets and serves as a strong baseline for the H₂O-3D dataset. We evaluate the pose estimation accuracy with different output representations and show that even when not using camera intrinsics, our method outperforms previous methods that require camera intrinsics. Our ablation study proves the importance of multi-scale feature sampling and keypoint-joint association stages and how it drives the pose estimator towards more accurate results.

2. Related Work

Many approaches have already been proposed for hand or object pose estimation from either RGB images or depth maps. Here we focus mainly on works that propose estimating hand poses during interactions *i.e.* hand-hand or hand-object interactions. We also discuss recent advances in transformer architectures in computer vision problems as they are highly relevant to our work.

2.1. Interacting Hand Pose Estimation

Hand pose estimation methods can be broadly classified as generative, discriminative, or hybrid approaches. Generative methods [35, 34, 36, 26, 52, 11] fit a parametric hand model to an observed image or depth map by minimizing a fitting error under some constraints. Discriminative methods [37, 49, 61, 14, 13, 21, 6, 31] have increasingly become popular with the success in deep learning and mostly directly predict the hand pose from a single frame. Generative methods often rely heavily on tracking and are prone to drift whereas discriminative methods tend to generalize poorly to unseen images [1]. Hybrid approaches [4, 47, 51, 45, 48, 32, 55, 7, 12, 43, 54] try to combine the best of these two worlds by using discriminative methods to detect visual cues in the image followed by model fitting.

Earlier methods [34, 26, 35] for generative hand pose estimation during interaction used complex optimization methods to fit a parametric hand model to RGBD data from one or more views. [36, 52] reconstruct the object model during in-hand scanning while continuously tracking the hand in a RGBD camera setup. [11] proposed multi-frame optimization to fit hand and object models to RGBD data from multiple RGBD cameras. Generative methods alone often lose tracking during close interactions or occlusions and are hence combined with discriminative methods to guide the optimization.

[4, 51] detect the fingertips as discriminative points and used them in the optimization along with a collision term

and physical modelling. Recently, [43] proposed high-fidelity hand surface tracking of hand-hand interactions in a multi-view setup where the regressed 3D hand joint locations were used for initializing the tracking. [54, 32, 12, 37, 7] compute dense features or keypoints from a single RGB or depth image and fit a hand model [41] to these estimates with physical constraints and joint angle constraints. Fully discriminative methods [49, 14, 31, 13] jointly estimate the 3D joint locations or hand model parameters of both the interacting hands or the interacting hand and the object by incorporating contacts and inter-penetrations in the training. [21] estimates the hand-object surface using implicit representation that naturally allows modelling of the contact regions between hand and object.

By contrast with the above mentioned approaches designed specifically for hand-hand or hand-object interaction scenarios, we propose in this work a unified discriminative approach for all hand interaction scenarios. Further, many previous methods perform poorly during close hand interactions due to similarity in appearance of the joints. In this work, we model relationship between all detected joints in the image resulting in more accurate pose estimation.

The success of discriminative methods depend on the variability of training data and several hand interaction datasets have been proposed. [10] first provided a marker-based hand-object interaction dataset using RGBD cameras. [61] proposed a RGB dataset with many hand-object interaction images but annotated only with the 3D poses for the hand. [11] and [14] respectively proposed real and synthetic hand-object interaction dataset with a single hand manipulating an object.

Recently, [31] developed a large-scale two-hand interaction dataset using semi-automatic annotation process. [46] used MoCap data to obtain a dataset of full body pose along with object pose during interaction and showed that such dataset can be used to generate realistic grasp pose on unseen objects. [6] used infrared cameras to identify single and two-hand contact regions on object and developed a markerless static hand-object interaction dataset with accurate contact annotations.

In this work, we also introduce a challenging two-hands-and-object interaction dataset which we created using the optimization method of [11]. Our dataset is made of videos of two hands from different subjects manipulating an object from the YCB dataset [56], annotated with the 3D poses of the hands and the object. Our architecture already performs well on this dataset and constitutes a strong baseline.

2.2. Transformers in Computer Vision

Transformers have recently been increasingly gaining popularity for vision related problems [22]. Features are often extracted from a CNN backbone and different architectures have been proposed to solve object detection [8, 59],

image classification [9], pose estimation [28, 17] and low-level image tasks [57, 25]. We refer the reader to [22] for a detailed survey.

[8] proposed to combine a CNN backbone with a Transformer to detect objects in an image. [59] further improved [8] by using multi-scale features from the CNN backbone and restricted the attention to only a small set of features from sampled locations. [28] proposed to reconstruct the vertices of a single human body or hand from an RGB image using multiple Transformer encoder layers and achieved state-of-the-art performance. [17] estimated a 3D pose from hand point-cloud data using a Transformer encoder-decoder architecture and proposed to generate query embeddings from input point-cloud instead of learning them as in [8, 59]. Different from these previous architectures, our method samples multi-scale image features from keypoint locations and uses a Transformer encoder-decoder architecture to estimate 3D pose of interacting hands and object from the sampled features.

3. Method

As shown in Fig. 2, our architecture first detects keypoints that are likely to correspond to the 2D locations of hand joints and encodes them as input to a transformer encoder. Using the transformer decoder, we predict pose parameters relative to each joint of both hands, plus additional parameters such as the translation between the hands and hand shape parameters. We also consider an auxiliary loss on the encoder to recognize the keypoints. Although this loss is not needed in principle, it guides the transformer decoder towards selecting more appropriate features and significantly improving the pose accuracy.

We detail below the keypoint detection and encoding step, how we use the transformer to predict the hands poses from these keypoints, the representations we considered for the 3D hand poses, and the auxiliary loss applied to the encoder.

3.1. Keypoint Detection and Encoding

Given the input image, we first extract keypoints that are likely to correspond to 2D hand joint locations. To do this, we predict a heatmap \mathcal{H} from the input image using a standard U-Net architecture, and we keep its local maximums. At this stage, we do not attempt to recognize which keypoint corresponds to which joint as it is a difficult task, and the predicted heatmap has only one channel. In practice, we keep a maximum of N_{hand} keypoints, with $N_{\text{hand}} = 64$, while the number of hand joints is 42 in total for 2 hands. The 2D keypoint locations are normalized to $[0, 1]$ range.

For training, we compute the ground truth heatmap \mathcal{H}^* by applying a 2D Gaussian kernel at each of the ground truth joint locations and minimize the L2 loss between this ground truth and the predicted heatmap to learn to predict

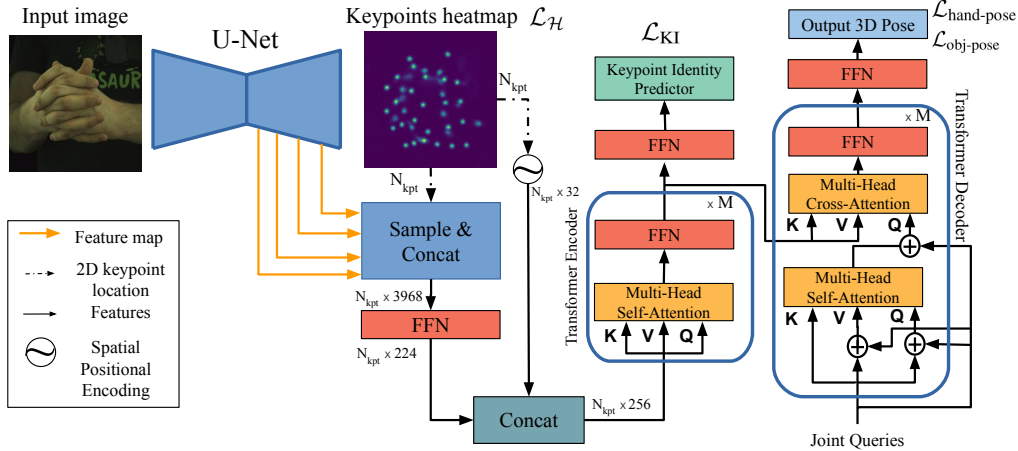


Figure 2: Overview of our approach. We detect the joints as keypoints, encode their appearances and 2D locations to give them as input to the transformer decoder. Despite the fact that some keypoints may be incorrect and not all the joints may be detected as keypoints, the transformer decoder can predict the hands poses. More details can be found in the text.

it:

$$\mathcal{L}_H = \|\mathcal{H} - \mathcal{H}^*\|_2^2. \quad (1)$$

The encoder of our U-Net [42] architecture is a ResNet [15] up to $C5$ layer as a backbone, followed by upsampling and convolutional layers with skip connections forming the decoder. We use 256×256 input image resolution and a heatmap resolution of 128×128 pixels.

We then compute for each detected keypoint an appearance and spatial encoding to represent the keypoints as input to the transformer. As shown in Fig. 2, for the appearance part, we extract image features from the decoder of the U-Net. More exactly, we sample feature maps at multiple layers of the U-Net decoder at the normalized keypoint locations using bilinear interpolation and concatenate them to form a 3968-D feature vector, which is then reduced down to 224-D encoding vector using a 3 layer MLP. For the spatial encoding, we obtain 32-D sine positional encoding similar to [8] corresponding to the 2D location of the keypoint. We finally concatenate the appearance and spatial encodings to form a 256-D vector representation of the keypoint.

Note that the non-maximum suppression operation to extract the keypoints is non-differentiable and thus the gradients do not flow through the peak detection operation while training.

3.2. Using a Transformer to Predict a 3D Pose from the Keypoints

For each keypoint K_i , we have now an encoding vector \mathcal{F}_i . We use these vectors as input to the encoder part of a transformer. The self-attention modules [53] of the encoder model the relationship between the keypoints and create global context-aware features that help the transformer associate each keypoint with a hand joint. To help the encoder model such relationships, we also consider an aux-

iliary joint association loss that will be detailed in Section 3.4. The transformer decoder predicts the 3D poses of the joints using learned joint queries. We detail which representations we use exactly for the 3D poses and their corresponding loss functions in Section 3.3.

Unlike previous works [8, 59, 17] where the learned queries input to the transformer decoder represent positional embedding, our learned queries embed the joint *identities*. As in a standard non-autoregressive transformer decoder [8, 59, 17, 18], the joint queries are transformed through a series of self-attention and cross-attention modules in the decoder. For each joint query, the cross-attention module in the decoder *soft-selects* the encoder features that best represent the joint being queried and transforms them. The transformed features are then fed to an MLP with 2 layers and a linear projection layer to predict joint-related pose parameters. Similar to [8], the pose is predicted after each decoder layer using MLPs with shared weights.

Along with the joint queries, we use an additional learned query to predict:

- the relative translation $T_{L \rightarrow R}$ between the hands;
- the 10-D MANO hand shape parameters β ;
- the weak perspective camera model [5, 20] parameters (scale $s_c \in \mathbb{R}^+$ and 2D translation $t_c \in \mathbb{R}^2$). This model projects a 3D point M into a 2D point m as $m = s_c \Pi(M) + t_c$, where $\Pi(M)$ is the orthographic projection. We use this projection for a loss term during training as explained below and its predicted parameters for visualization of the predicted poses.

We do not use specific loss terms for these predictions, but they are used in the estimation of poses. In the next subsection, we provide details about the different representations we consider for the 3D hand poses and their corresponding losses.

3.3. Hand Pose Representations and Losses

As noted in previous works [13, 20, 40, 39, 14], regressing 3D joint locations directly is more accurate (in terms of joint error) than regressing model parameters such as the MANO joint angles. However, regressing MANO joint angles provides access to the complete hand mesh required for modeling contacts and interpenetration during interactions [46, 6, 14] or for learning in a weakly supervised setup [24, 3, 13], which could be interesting for future extension of our method. We therefore consider both options (3D joint locations and joint angles) as outputs and show later in our experiments that our architecture enables joint angle representation to achieve competitive performance when compared to the joint location representation. For the 3D joint hand locations, we consider two types of representations: parent-relative joint vectors and parent-relative 2.5D pose. We detail the three possible representations and their corresponding losses below.

Parent-relative joint vectors \hat{V} . In this representation, each joint j is associated with a 3D ‘joint vector’ V_j given by $V_j = J_{3D}(j) - J_{3D}(p(j))$, where J_{3D} is the 3D joint location and $p(j)$ refers to the parent joint index of joint j . The advantage of this representation is that it defines the hand pose relative to its root without requiring knowledge of the camera intrinsics. We estimate 20 joint vectors per hand using 20 joint queries, from which we can compute the root-relative 3D location of each joint by simple accumulation. The root-relative 3D pose of the left hand is translated by the predicted right-hand relative translation $T_{L \rightarrow R}$, resulting in right hand root-relative 3D joint locations. In total we use 40 joint queries (20 per hand) and one additional query to estimate $T_{L \rightarrow R}$ and weak camera parameters.

When using this representation, we supervise our architecture using a pose loss $\mathcal{L}_{\text{hand-pose}}^V$ that combines 3 loss terms:

$$\mathcal{L}_{\text{hand-pose}}^V = \mathcal{L}_V + \mathcal{L}_{3D} + \mathcal{L}_{2D}, \quad (2)$$

where \mathcal{L}_V is the L1 loss between the predicted joint vectors and their ground truth, \mathcal{L}_{3D} is the L1 loss between the 3D joint locations retrieved by summing the predicted joint vectors and their ground truth, and \mathcal{L}_{2D} is the L1 loss between the reprojections of the 3D joint locations using the predicted scale \hat{s}_c and 2D translation \hat{t}_c and their ground truth locations.

Parent-relative 2.5D pose [19, 31]. In this representation, each joint is parameterised by its 2D location J_{2D} , and the difference ΔZ^p between its depth and the depth of its parent. The camera intrinsics matrix K and the absolute depth Z_{root} of the root joint (the wrist) [31] or the scale of the hand [19] are then required to reconstruct the 3D pose of the hand in camera coordinate system as $J_{3D} = K^{-1} \cdot (Z_{\text{root}} + \Delta Z^r) \cdot [J_{2D_x}, J_{2D_y}, 1]^T$, where ΔZ^r is the root-relative depth of the joint computed from

its predicted ΔZ^p and the predicted ΔZ^p for its parents. J_{2D_x}, J_{2D_y} are the predicted x and y coordinates of J_{2D} .

When using this representation, we also predict the root depth Z_{root} separately using RootNet [29] as in [31]. In total we use 42 joint queries (21 per hand) and an additional query to estimate $T_{L \rightarrow R}$. We supervise our architecture using a pose loss $\mathcal{L}_{\text{hand-pose}}^{2.5D}$ that combines three loss terms:

$$\mathcal{L}_{\text{hand-pose}}^{2.5D} = \mathcal{L}'_{2D} + \mathcal{L}_Z + \mathcal{L}_T, \quad (3)$$

where \mathcal{L}'_{2D} is the L1 loss between the predicted 2D locations of the joints and their ground truth, \mathcal{L}_Z is the L1 loss between the predicted ΔZ^p and their ground truth and \mathcal{L}_T is the L1 loss between the predicted $T_{L \rightarrow R}$ and its ground truth.

MANO joint angles [41]. In this representation, each 3D hand pose is represented by 16 3D joint angles in the hand kinematic tree and is estimated using 16 queries per hand. The MANO hand shape parameter, the relative translation between the hands and the weak camera model parameters are estimated by an additional query resulting in a total of 33 queries. Such a pose representation enables obtaining differentiable 3D hand meshes [41] directly, which are essential if one wants to model contacts and interpenetration between hands and objects [13, 46, 6]. Given the predicted 3D joint angles θ for each hand, the predicted shape parameters β , and the predicted relative hand translation $T_{L \rightarrow R}$, it is possible to compute the 3D locations of each joint relative to the right hand root joint.

When using this representation, we supervise our architecture using a pose loss $\mathcal{L}_{\text{hand-pose}}^{\text{MANO}}$ that combines 3 loss terms:

$$\mathcal{L}_{\text{hand-pose}}^{\text{MANO}} = \mathcal{L}'_{3D} + \mathcal{L}_\theta + \mathcal{L}_{2D}, \quad (4)$$

where \mathcal{L}'_{3D} is the L1 loss between the 3D joint locations computed from the predicted 3D joint angles and MANO shape parameters, and their ground truth. \mathcal{L}_θ is the L1 loss between the predicted 3D joint angles and their ground truth, and behaves as a regularizer to avoid unrealistic poses. \mathcal{L}_{2D} is the L1 loss between reprojections of the computed 3D joint locations and their ground truth using the predicted parameters for the weak projection model, as in Eq. (2).

3.4. Keypoint-Joint Association

In addition to the losses introduced above, we also rely on an auxiliary loss for predicting the keypoint identities by the transformer encoder, *i.e.* we predict for each keypoint to which hand and joint it corresponds. As we show in our experiments, this loss allows the joint queries to select more appropriate features from the transformer encoder during cross-attention, leading to significant increase in accuracy of the pose estimates.

The identity of the keypoints are predicted using an MLP prediction head consisting of 2 fully connected layers, a linear projection layer and a softmax layer. Similar to the pose

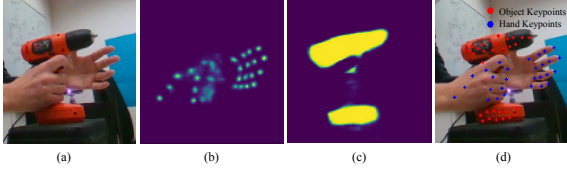


Figure 3: Keypoint detection in a hand-object image (a). We train the U-net decoder to output hand keypoints heatmap (b) and object segmentation map (c). The hand keypoints and object keypoints are detected from heatmap and segmentation map, respectively as shown in (d).

prediction heads on the decoder, the keypoint identity prediction heads are attached after each encoder layer and the weights of the MLPs are shared. We use a standard cross-entropy loss over all keypoints:

$$\mathcal{L}_{\text{KI}} = \sum_i \text{CE}((h_i, j_i), (h_i^*, j_i^*)), \quad (5)$$

where (h_i, j_i) are the hand (left or right) and the joint index predicted for keypoint i and (h_i^*, j_i^*) their ground truth. CE represents the cross-entropy loss. The predictions can result in multiple keypoints assigned to the same joint identity, but as mentioned above, their purposes are only to guide the joint queries to find appropriate features for pose estimation. To obtain the ground truth identity for the detected keypoints, we associate them at training time with the closest reprojection of a ground truth 3D joint, if the distance is below a threshold γ . If there are no joints within a distance of γ , the keypoint is assigned to the background class. We set $\gamma = 3$ in our experiments.

3.5. Object Pose Estimation

The method presented above can generalize easily to also predict the 3D pose of an object. As done in previous works [13, 49], we assume the 3D model of the object is available. Along with predicting the heatmap for the hand keypoints, as shown in Fig. 3, we also predict a segmentation map of the object by adding an additional prediction head to the U-Net decoder. We then randomly select $N_{\text{obj}} = 20$ points from this segmentation map and refer to them as ‘object keypoints’. Alternatively, we also tried estimating the heatmap of 2D reprojections of fixed points on the object mesh and selecting their local maximums as object keypoints and obtained similar results. We encode the object keypoints in a 256-D vector, exactly like the hand keypoints. Collectively, these keypoint encodings cover the object appearance, and it will be possible to compute the 3D rotation and translation of the object from them. As illustrated in Figure 3, the encodings of N_{obj} object keypoints and N_{hand} hand keypoints are provided *together* to the transformer encoder.

Along with the joint queries that estimate the hand pose, we consider 2 additional queries to the decoder for predict-

ing the 3D object rotation and 3D object translation relative to the right hand. We parameterize the object rotation using the method proposed in [58] and used in particular in [27]. On the encoder side, similar to predicting the joint identities of the hand keypoints from their features, we also predict if a keypoint belongs to the object or not, allowing the transformer decoder to further differentiate between hand and object features during cross-attention.

We use a symmetry-aware object corner loss similar to [38] to train the network and is defined as,

$$\mathcal{L}_{\text{obj-pose}} = \min_{R \in \mathcal{S}} \frac{1}{8} \sum_{i=1}^8 \|\hat{P} \cdot B_i - P^* \cdot R \cdot B_i\|_2^2, \quad (6)$$

where \hat{P} and P^* denotes the estimated and ground-truth object pose matrix, B_i , the i^{th} 3D bounding box corner of the object in rest pose and \mathcal{S} the set of rotation matrices, which when applied to the object, does not change its appearance.

3.6. End-to-End Training

We train our architecture end-end by minimizing the sum of the losses introduced above:

$$\mathcal{L} = \mathcal{L}_{\mathcal{H}} + \mathcal{L}_{\text{KI}} + \mathcal{L}_{\text{hand-pose}} + \mathcal{L}_{\text{obj-pose}}, \quad (7)$$

where $\mathcal{L}_{\text{hand-pose}}$ is the loss on hand poses depending on the output representation as discussed in Section 3.3. During the initial few epochs when the estimated keypoint heatmap is less accurate, we use the ground truth 3D joint reprojections and ground truth object segmentations for obtaining keypoint locations and later switch to the predicted heatmap and segmentations. We use a 256×256 pixel image patch loosely cropped around the hand and object as input to the network and use Adam [23] optimizer with a learning rate of 10^{-4} and 10^{-5} for transformer and backbone, respectively. We train the network for 50 epochs on 3 Titan V GPUs with a total batch size of 78 and use on-line augmentation techniques such as rotation, scale and mirroring during training.

4. Evaluations

We evaluated our method on three challenging hand interaction datasets: InterHand2.6M, HO-3D, and our H₂O-3D dataset. We discuss them below.

4.1. InterHand2.6M

Training and test sets. InterHand2.6M [31] is a recently published two-hand interaction dataset with many challenging poses. It was annotated semi-automatically and contains 1.2 million images in its initial release (V0.0). We use the automatically annotated training images (497K images) from this dataset as many manually annotated images have annotations for only one of the two hands. We evaluate our method on the automatically annotated test set of 286K images.

	Camera Intrinsics	MPJPE (mm)			MRRPE (mm)
		Single Hand	Inter. Hand	All	
InterNet [31]	Yes	13.79	21.24	17.54	40.46
Joint Vec.	No	12.42	17.08	14.76	33.14
Joint Ang.*	No	14.00	19.16	16.61	37.91
Joint Ang.	No	15.36	20.61	18.01	37.91
2.5D Pose	Yes	11.73	17.69	14.73	34.40

Table 1: **Accuracy of our method with 3 different pose representations on InterHandV0.0.** Our method achieves 16% higher accuracy than [31] which relies on a fully CNN architecture. Even while estimating MANO [41] joint angles our method outperforms [31] which estimates 3D joint locations directly. * indicates ground-truth 3D joints obtained from fitted MANO models.

Metrics. As was done in [31] for evaluating their baseline, we consider the Mean Per Joint Position Error (MPJPE) and the Mean Relative-Root Position Error (MRRPE). MPJPE computes the Euclidean distance between the predicted and ground truth 3D joint locations after root joint alignment and indicates the accuracy of root-relative 3D pose. The alignment is carried out separately for the right and the left hands. MRRPE evaluates the accuracy of the localization of the left hand relative to the right hand.

Results. Table 1 compares the accuracy of our method using one of the different hand pose representations described in Section 3.3. We also compare with InterNet [31], which uses a CNN architecture to predict the 2.5D pose representation of both hands. We refer the reader to Fig. 4 and the suppl. mat. for more qualitative results.

When predicting the 2.5D pose representation similar to [31], our method outperforms [31] in both single hand and interacting hand scenarios. The improvement is more significant (17%) in the case of the interacting hands scenario, thus demonstrating that transformer performs better than a CNN in capturing joint-to-joint relationships.

The parent-relative joint vector representation which does not require camera intrinsics to reconstruct root-relative pose also outperforms [31] which requires camera intrinsics and is slightly less accurate than the 2.5D pose representation. Another interesting observation from Table 1 is that the joint angle representation performs similar to [31], which outputs directly the 3D joint locations. Note that the fitted MANO models to ground-truth 3D joint locations provided by [31] themselves have a mean joint error of 5mm indicating the lower bound for errors when estimating joint angles. As previous works [40, 39, 14, 13, 20] that use CNN architecture have reported, regressing joint angles or its PCA components is harder than directly estimating 3D joint locations. Our CNN-transformer architecture performs competitively even when regressing joint angles.

4.2. HO-3D

Training and test sets. The HO-3D [11] dataset contains hand-object interaction sequences with only a right hand

	Camera Intrins.	Image Crop	Joint Err.	AUC		Must. Bottle*	Bleach Cleans.	Potted Meat.*	All
[14]	No	Yes	3.18	0.46	Ours- nosym	4.72	5.70	8.92	7.02
[13]	Yes	No	3.69	0.37	Ours- sym	4.41	6.03	9.08	7.20
Ours	No	Yes	2.57	0.54					

(a)

(b)

Table 2: **Accuracy of our method on HO-3D [11]. All errors in cm.** (a) Hand 3D pose accuracy using mean joint error metric. Our method achieves state-of-the-art results. (b) Object 3D pose accuracy. Our method trained without symmetry-aware loss (‘Ours-nosym’) outperforms [13] which also does not consider object symmetry. ‘Ours-sym’ corresponds to results with symmetry-aware loss. * represents symmetric object.

and one among 10 objects from YCB [56]. It contains 66K training images and 11K test images with automatically obtained annotations. HO-3D test set contains 3 seen objects and one object used in the training data. We consider only the seen objects for evaluation.

Metrics. As in [11], we report the mean joint error after scale-translation alignment of the root joint and the area-under-the-curve (AUC) metrics to evaluate the hand pose. The object pose is computed w.r.t to the hand frame of reference. To evaluate the object pose, we use the standard Maximum Symmetry-Aware Surface Distance (MSSD) metric as defined in [16]. MSSD considers the symmetry of objects and we provide details about the angles and axes of symmetry for different objects in HO-3D in the suppl. mat.

Results. We estimate the hand pose using the parent-relative joint vector representation and object pose relative to the hand. We use 20 joint queries for hand pose, 1 query for weak camera model parameters and 2 queries for object pose.

Table 2a compares the accuracy of the proposed hand pose estimation method with other approaches and shows that our method achieves state-of-the-art performance, faring significantly better than previous methods. Table 2b compares the accuracy of the estimated object poses with [13]. [13] estimates the object pose using a CNN backbone followed by fully connected layers that regress the object rotation (using an axis-angle representation) and object translation in the camera coordinate system. As [13] does not handle the fact that some objects are symmetrical during training, we show results with (‘Ours-sym’) and without (‘Ours-nosym’) handling symmetry in training. Our method obtains more accurate hand-relative object poses. We show some qualitative results in Fig. 5 and suppl. mat.

4.3. H₂O-3D

Training and test sets. We introduce a dataset named H₂O-3D comprising sequences of two hands manipulating an object automatically annotated with the 3D poses of the



Figure 4: **Qualitative results on InterHand2.6M [31].** Our method obtains accurate poses of hands during complex interactions. We show different views of MANO mesh.

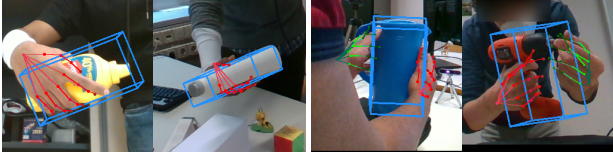


Figure 5: **Qualitative results of our method on HO-3D (first two) and H₂O-3D (last two) datasets.** Our method recovers poses even under strong occlusion from the object and achieves state-of-the-art results on HO-3D while serving as a strong baseline for H₂O-3D.

hands and the object, by extending the work of [11] to consider two hands. In this dataset, six different subjects manipulate 10 different objects from YCB using both hands. We captured 50K training images and 12K test images using a multi-view setup with 5 RGBD cameras. H₂O-3D test set contains 3 objects seen in the training set. More details are provided in the suppl. mat. H₂O-3D is more challenging than previous hand interaction datasets as there are many large occlusions between the hands and the objects.

Metrics and Results We use the MPJPE and MRRPE metrics (see Section 4.1) for the hand and the MSSD metric for the object (see Section 4.2). We estimate the parent-relative joint vector representation of the 2 hand poses (40 joint queries), right hand relative translation of the left hand (1 query) and right hand relative object pose (2 queries) with a total of 43 queries at the transformer decoder. We also used HO-3D train split and mirrored the images randomly during training to obtain right hand- and left hand-only images, to later combine with the training set of H₂O-3D.

Our method achieves a MPJPE of 2.84 cm and a MRRPE of 9.08 cm on this dataset. Due to large mutual occlusions, estimating the translation between the hands is more challenging and the MRRPE is 2.5 times worse than on InterHands2.6M which does not contain objects. On objects, our method achieves MSSD values of 15.29 cm with object specific MSSD values of 7.83 cm, 9.68 cm and 21.52 cm for ‘Power Drill’, ‘Bleach Cleanser’ and ‘Pitcher Base’, respectively. The large error for the non-symmetric ‘Pitcher Base’ object is mainly due to the limitation of our method to identify the ‘handle’ which is crucial to disambiguate the poses, thus resulting in inaccurate rotation along the z-axis of the estimated poses for the ‘Pitcher Base’. We show some qualitative results in Fig. 5 and the supplementary material.

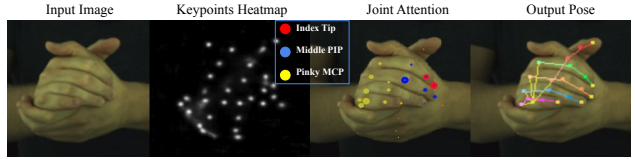


Figure 6: **Visualizing the cross-attention for three joint queries of the right hand:** Index fingertip (red), middle PIP (blue) and pinky MCP joints (yellow). For each joint query, the corresponding colored circles in the third image indicates the locations of the keypoints attended by the query. The radius of the circle is proportional to the attention weight. We observe that each joint query select image features from the respective joint location.

	MPJPE (mm)			MRRPE(mm)
	Single Hand	Inter. Hand	All	
Ours w/o \mathcal{L}_{KI}	14.63	22.25	18.47	46.81
DETR [8]-style	15.25	20.86	18.07	39.08
Ours	12.42	17.08	14.76	33.14

Table 3: **Ablation study on InterHand2.6M.** The keypoint identity loss \mathcal{L}_{KI} increases the accuracy of pose estimation by 20%. The DETR [8]-style architecture uses features only from the last layer of the U-Net encoder, which is a low-resolution feature map, resulting in inferior performance.

5. Ablation Study

Comparison with CNN architecture As we show in Table 1, our CNN-Transformer architecture outperforms the CNN-only architecture of [31] by a large margin (16%). The explicit modeling of the relationship between the image features at only keypoint locations allows our architecture to attain better accuracy.

Visualization of attention To understand which features of the encoder are attended by a given joint query at the decoder, we visualize the cross-attention weights for three joint queries of the right hand in Fig. 6. The joint queries learn to attend to the keypoint features that mostly correspond to the respective joint location in the image.

How important is the keypoint identity loss? Table 3 (‘Ours w/o \mathcal{L}_{KI} ’) shows the effect of not using the keypoint identity prediction loss in the transformer encoder. This loss helps the architecture to not confuse the joints and results in 20% higher accuracy.

How important is multi-scale feature sampling? In Table 3, we compare our method with a DETR [8]-style architecture which uses low-resolution feature map at the last layer of U-Net encoder as input tokens to the transformer. More details about this architecture are provided in the supplementary material. Our architecture which uses multi-scale feature map sampling achieves 18% higher accuracy.

Supplementary Material

In this supplementary material, we discuss the limitations of our method, provide more details about the experiments and also show several qualitative results and comparisons. We also refer the reader to the **Supplementary Video** for visualization of results on different action sequences.

A. H₂O-3D Dataset

Our dataset contains two-hands + object interaction sequences captured on a multi-view setup with 5 RGBD cameras. We collect data from six different subjects and consider ten objects from the YCB dataset with each subject manipulating the object with a functional intent. The dataset is automatically annotated with 3D poses of hands and objects using the optimization method of [11]. The dataset in total contains 50K training images and 12K test images from 20 different sequences. We show some sample annotations from the dataset in Fig. 7. Tab. 4 shows the list of YCB objects that are considered symmetric during our training along with their axis and angle of symmetry.

B. Method Limitations

Though our method results in accurate poses during interactions, the results are sometimes not plausible as we do not model contacts and interpenetration [21, 6, 14] between hands and objects. Further, during highly complex and severely occluded hand interactions as we show in last row of Fig. 10, our method fails to obtain reasonable hand poses. We believe these problems can be tackled in the future by incorporating temporal information and physical modeling into our architecture.

C. Qualitative Results and Comparisons

We provide more qualitative results on HO-3D, H₂O-3D and InterHand2.6M.

C.1. HO-3D and H₂O-3D Qualitative Results

Fig. 8 shows qualitative results on H₂O-3D and HO-3D. Note that as we do not model contacts and interpenetration between hands and object, our method sometimes results in implausible poses as we show in the last example of Fig. 8.

Object	Axis	Angle
Mustard Bottle	Z	180°
Cracker Box	X,Y,Z	180°, 180°, 180°
Sugar Box	X,Y,Z	180°, 180°, 180°
Potted Meat Can	X,Y,Z	180°, 180°, 180°
Bowl	Z	∞

Table 4: Objects and their axes of symmetry used for training on HO-3D and H₂O-3D datasets.

C.2. InterHand2.6M Qualitative Results

Fig. 9 compares the estimated poses using the InterNet method from [31] and our proposed approach. InterNet is a fully-CNN architecture which outputs poses in 2.5D representation and we show our results using joint vector representation. As noted in Section 1 and Table 3 of the main paper, fully-CNN approaches do not explicitly model the relationship between image features of joints and tend to *confuse* joints during complex interactions. Our method performs well during complex interactions and strong occlusions (see last row of Fig. 9).

We show more qualitative results using the MANO angle representation in Fig. 10. Our retrieved poses are very similar to ground-truth poses. As we show in the last row of Fig. 10, our method fails during scenarios where the hand is severely occluded during complex interaction.

D. DETR [8]-style network architecture

The DETR [8] style architecture discussed in Table 4 of the main paper provides the feature map at the output of U-Net encoder (see Fig. 1 of the main paper) to the transformer. The U-net encoder features are 2048-D with a 8×8 spatial resolution and are converted to 224-D using 3 MLP layers. To be consistent with our architecture, we concatenate these features with 32-D positional embeddings resulting in 256-D features and keep the rest of the transformer architecture identical, resulting in the same number (64) of input tokens to the Transformer as our proposed architecture. We train the DETR-style network for 50 epochs with a total batch size of 78 on 3 TitanV GPUs and a learning rate of 10^{-4} and 10^{-5} for transformer and backbone, respectively.

E. Attention Visualization

In Fig. 11 we show more visualization of the cross-attention weights for six different joint queries. More specifically, the cross-attention weights represent the multiplicative factor on each of the encoder features for a given joint query in the decoder. As the encoder features are essentially transformed image features at detected keypoint locations, the visualizations in Fig. 11 represent the contribution of image features from different locations in estimating the joint-related parameter. We observe that the decoder learns to select image features from respective joint locations for each query.

References

- [1] Anil Armagan, Guillermo Garcia-Hernando, Seungryul Baek, Shreyas Hampali, M. Rad, Zhaohui Zhang, Shipeng Xie, Ming xiu Chen, Boshen Zhang, F. Xiong, Yang Xiao, Zhiguo Cao, J. Yuan, Pengfei Ren, Weiting Huang, Haifeng Sun, M. Hruz, J. Kanis, Z. Krnoul, Qingfu Wan, S. Li, Linlin

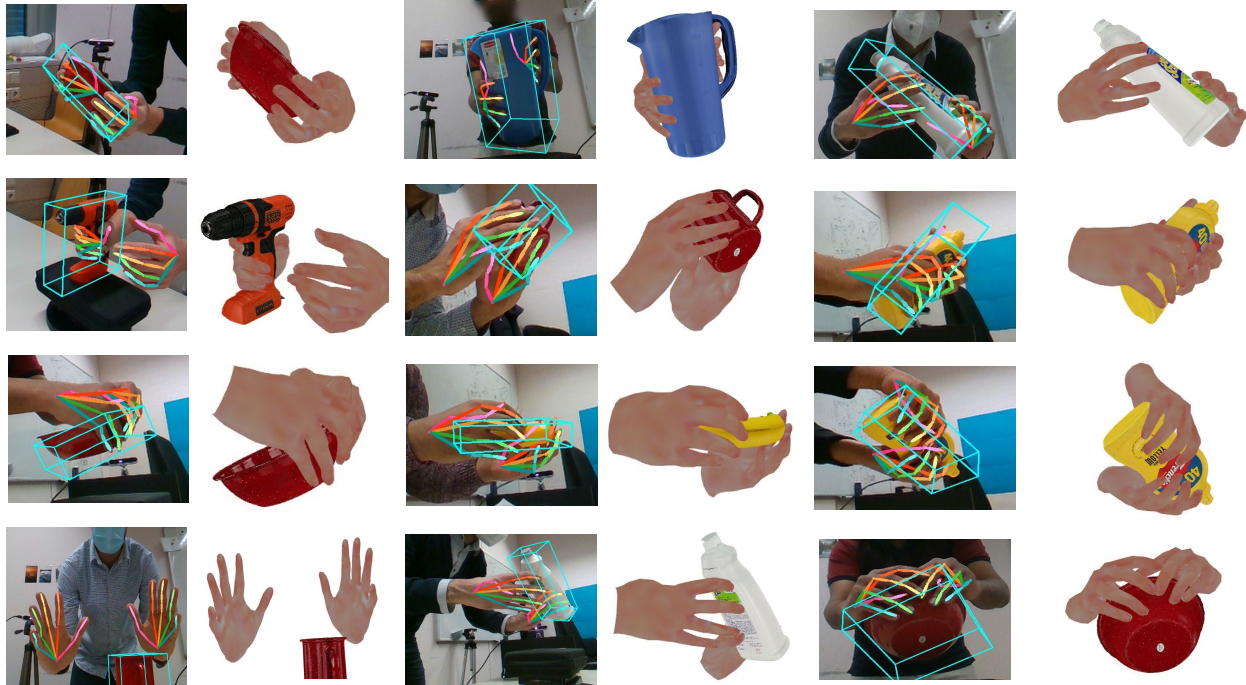


Figure 7: Samples from H₂O-3D dataset. Our dataset contains sequences with complex actions performed by both hands on YCB [56] objects.



Figure 8: Qualitative results on H₂O-3D and HO-3D [11]. Our method obtains state-of-the-art results on HO-3D while predicting reasonable results on H₂O-3D. The last example is a failure case where the predicted relative translations are inaccurate.

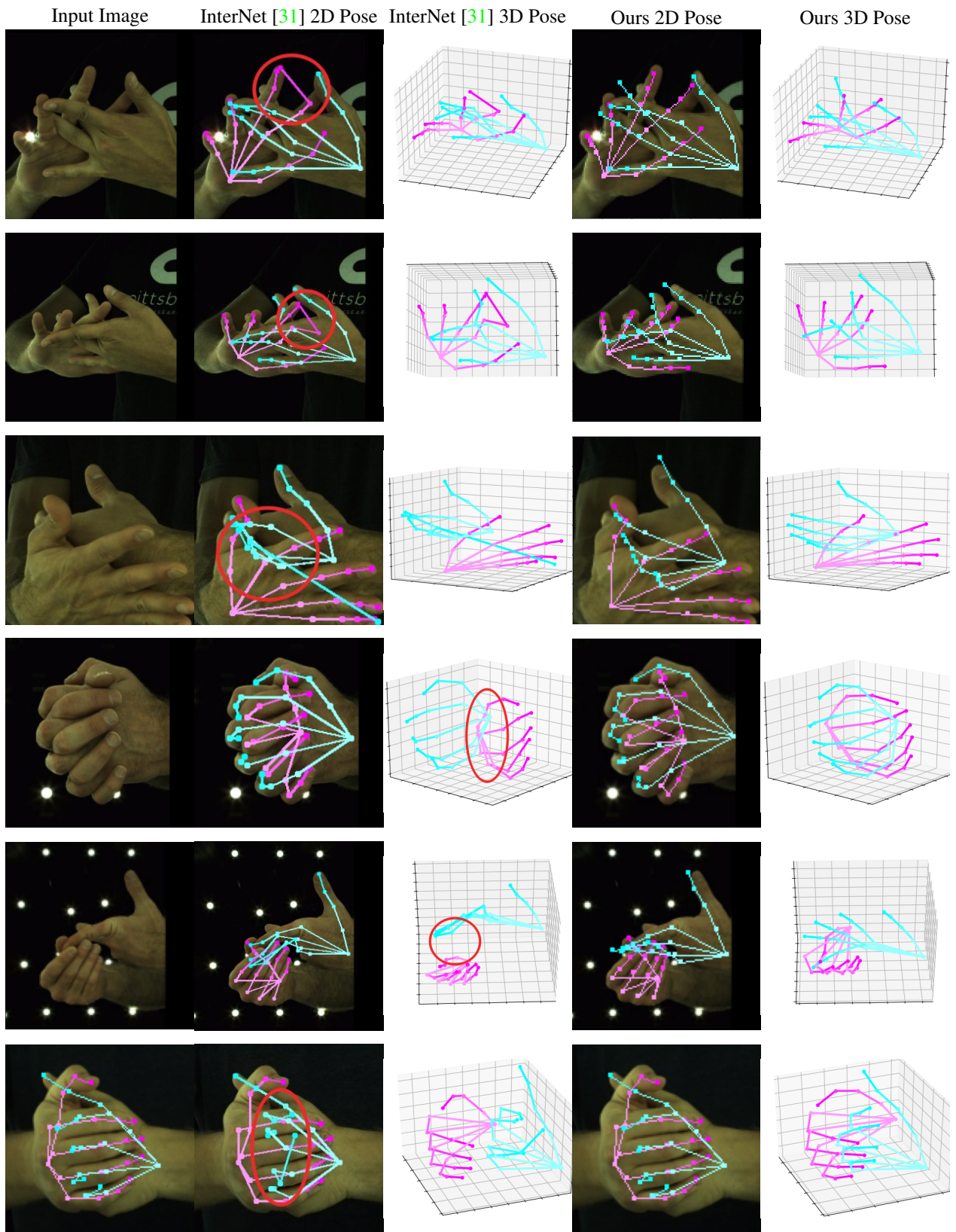


Figure 9: Qualitative comparison between InterNet [31] and our proposed method. Our method outputs more accurate poses even during strong occlusions. Red circles indicate regions where InterNet results are inaccurate.



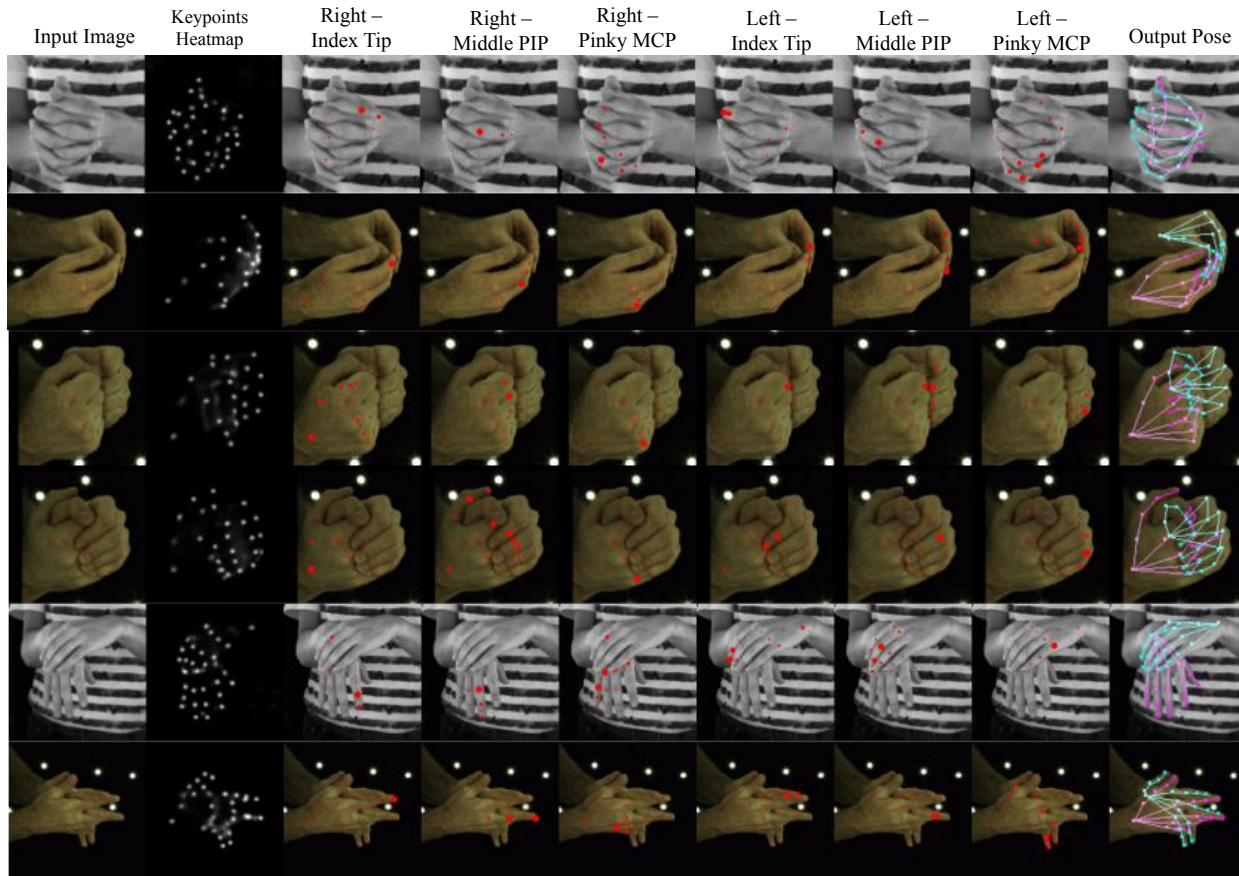


Figure 11: Attention visualization for 6 joint queries. Each joint query attends to the image feature from the respective joint location.

- Yang, Dongheui Lee, A. Yao, Weiguo Zhou, Sijia Mei, Yunhui Liu, A. Spurr, U. Iqbal, P. Molchanov, Philippe Weinzaepfel, Romain Brégier, Grégory Rogez, V. Lepetit, and T. Kim. Measuring generalisation to unseen viewpoints, articulations, shapes and objects for 3d hand pose estimation under hand-object interaction. In *ECCV*, 2020. 2
- [2] Seungryul Baek, K. Kim, and Tae-Kyun Kim. Pushing the envelope for rgb-based dense 3d hand pose estimation via neural rendering. In *CVPR*, pages 1067–1076, 2019. 1
- [3] Seungryul Baek, K. Kim, and Tae-Kyun Kim. Weakly-supervised domain adaptation via gan and mesh model for estimating 3d hand poses interacting objects. In *CVPR*, pages 6120–6130, 2020. 5
- [4] Luca Ballan, A. Taneja, Juergen Gall, L. Gool, and M. Pollefeys. Motion capture of hands in action using discriminative salient points. In *ECCV*, 2012. 2
- [5] Adnane Boukhayma, Rodrigo de Bem, and Philip H. S. Torr. 3d hand shape and pose from images in the wild. In *CVPR*, pages 10843–10852, 2019. 4
- [6] Samarth Brahmhatt, Chengcheng Tang, Christopher D. Twigg, Charles C. Kemp, and James Hays. Contactpose: A dataset of grasps with object contact and hand pose. In *ECCV*, 2020. 2, 3, 5, 9
- [7] Zhe Cao, Ilija Radosavovic, A. Kanazawa, and J. Malik. Reconstructing hand-object interactions in the wild. *ArXiv*, abs/2012.09856, 2020. 2, 3
- [8] Nicolas Carion, Francisco Massa, Gabriel Synnaeve, Nicolas Usunier, Alexander Kirillov, and Sergey Zagoruyko. End-to-end object detection with transformers. In *ECCV*, volume 12346, pages 213–229, 2020. 2, 3, 4, 8, 9
- [9] A. Dosovitskiy, Lucas Beyer, Alexander Kolesnikov, Dirk Weissenborn, Xiaohua Zhai, Thomas Unterthiner, M. Dehghani, Matthias Minderer, Georg Heigold, S. Gelly, Jakob Uszkoreit, and N. Houlsby. An image is worth 16x16 words: Transformers for image recognition at scale. *ArXiv*, abs/2010.11929, 2020. 2, 3
- [10] Guillermo Garcia-Hernando, Shanxin Yuan, Seungryul Baek, and Tae-Kyun Kim. First-person hand action benchmark with rgb-d videos and 3d hand pose annotations. In *CVPR*, pages 409–419, 2018. 3
- [11] Shreyas Hampali, Mahdi Rad, Markus Oberweger, and Vincent Lepetit. Honnotate: A method for 3d annotation of hand

- and object poses. In *CVPR*, 2020. [1](#), [2](#), [3](#), [7](#), [8](#), [9](#), [10](#)
- [12] Shangchen Han, B. Liu, R. Cabezas, Christopher D. Twigg, P. Zhang, Jeff Petkau, Tsz-Ho Yu, Chun-Jung Tai, Muzaffer Akbay, Z. Wang, Asaf Nitzan, G. Dong, Yuting Ye, Lingling Tao, Chengde Wan, and R. Wang. Megatrack: monochrome egocentric articulated hand-tracking for virtual reality. *ACM Trans. Graph.*, 39:87, 2020. [1](#), [2](#), [3](#)
- [13] Yana Hasson, Bugra Tekin, Federica Bogo, Ivan Laptev, Marc Pollefeys, and Cordelia Schmid. Leveraging photometric consistency over time for sparsely supervised hand-object reconstruction. In *CVPR*, 2020. [2](#), [3](#), [5](#), [6](#), [7](#)
- [14] Yana Hasson, Gül Varol, Dimitrios Tzionas, Igor Kalevatykh, Michael J. Black, Ivan Laptev, and Cordelia Schmid. Learning joint reconstruction of hands and manipulated objects. In *CVPR*, 2019. [1](#), [2](#), [3](#), [5](#), [7](#), [9](#)
- [15] Kaiming He, X. Zhang, Shaoqing Ren, and Jian Sun. Deep Residual Learning for Image Recognition. In *CVPR*, pages 770–778, 2016. [4](#)
- [16] Tomás Hodan, Martin Sundermeyer, Bertram Drost, Yann Labbé, Eric Brachmann, Frank Michel, Carsten Rother, and Jiri Matas. BOP challenge 2020 on 6d object localization. In *Computer Vision - ECCV 2020 Workshops - Glasgow, UK, August 23-28, 2020, Proceedings, Part II*, volume 12536, pages 577–594, 2020. [7](#)
- [17] Lin Huang, Jianchao Tan, Ji Liu, and Junsong Yuan. Hand-transformer: Non-autoregressive structured modeling for 3d hand pose estimation. In *ECCV*, pages 17–33, 2020. [2](#), [3](#), [4](#)
- [18] Lin Huang, Jianchao Tan, J. Meng, J. Liu, and J. Yuan. Hotnet: Non-autoregressive transformer for 3d hand-object pose estimation. *Proceedings of the 28th ACM International Conference on Multimedia*, 2020. [4](#)
- [19] Umar Iqbal, Pavlo Molchanov, Thomas Breuel, Juergen Gall, and Jan Kautz. Hand pose estimation via latent 2.5d heatmap regression. In *ECCV*, pages 125–143, 2018. [1](#), [5](#)
- [20] Angjoo Kanazawa, Michael J. Black, David W. Jacobs, and Jitendra Malik. End-to-end recovery of human shape and pose. In *CVPR*, pages 7122–7131, 2018. [4](#), [5](#), [7](#)
- [21] Korrawe Karunratanakul, Jinlong Yang, Yan Zhang, Michael J. Black, Krikamol Muandet, and Siyu Tang. Grasping field: Learning implicit representations for human grasps. *2020 International Conference on 3D Vision (3DV)*, pages 333–344, 2020. [2](#), [3](#), [9](#)
- [22] Salman Khan, Muzammal Naseer, Munawar Hayat, Syed Waqas Zamir, F. Khan, and M. Shah. Transformers in vision: A survey. *ArXiv*, abs/2101.01169, 2021. [2](#), [3](#)
- [23] Diederik P. Kingma and Jimmy Ba. Adam: A method for stochastic optimization. In *ICLR*, 2015. [6](#)
- [24] Dominik Kulon, Riza Alp Güler, I. Kokkinos, M. Bronstein, and S. Zafeiriou. Weakly-supervised mesh-convolutional hand reconstruction in the wild. In *CVPR*, pages 4989–4999, 2020. [5](#)
- [25] Manoj Kumar, Dirk Weissenborn, and Nal Kalchbrenner. Colorization transformer. *ArXiv*, abs/2102.04432, 2021. [2](#), [3](#)
- [26] Nikolaos Kyriazis and Antonis A. Argyros. Scalable 3d tracking of multiple interacting objects. In *CVPR*, pages 3430–3437, 2014. [2](#)
- [27] Yann Labbé, J. Carpentier, Mathieu Aubry, and Josef Sivic. Cosypose: Consistent multi-view multi-object 6d pose estimation. In *ECCV*, 2020. [6](#)
- [28] Kevin Lin, Lijuan Wang, and Zicheng Liu. End-to-end human pose and mesh reconstruction with transformers. In *CVPR*, 2021. [2](#), [3](#)
- [29] Gyeongsik Moon, Ju Yong Chang, and Kyoung Mu Lee. Camera distance-aware top-down approach for 3d multi-person pose estimation from a single rgb image. In *ICCV*, pages 10132–10141, 2019. [5](#)
- [30] Gyeongsik Moon and Kyoung Mu Lee. I2l-meshnet: Image-to-lixel prediction network for accurate 3d human pose and mesh estimation from a single rgb image. In *ECCV*, 2020. [1](#)
- [31] Gyeongsik Moon, Shoou-I Yu, He Wen, Takaaki Shiratori, and Kyoung Mu Lee. Interhand2.6m: A dataset and baseline for 3d interacting hand pose estimation from a single rgb image. In *ECCV*, 2020. [1](#), [2](#), [3](#), [5](#), [6](#), [7](#), [8](#), [9](#), [11](#), [12](#)
- [32] F. Mueller, M. Davis, F. Bernard, Oleksandr Sotnychenko, M. Verschoor, M. Otaduy, D. Casas, and C. Theobalt. Real-time pose and shape reconstruction of two interacting hands with a single depth camera. *ACM Transactions on Graphics (TOG)*, 38:1 – 13, 2019. [2](#), [3](#)
- [33] Markus Oberweger, Paul Wohlhart, and Vincent Lepetit. Training a feedback loop for hand pose estimation. In *ICCV*, pages 3316–3324, 2015. [1](#)
- [34] I. Oikonomidis, N. Kyriazis, and A. A. Argyros. Full dof tracking of a hand interacting with an object by modeling occlusions and physical constraints. In *ICCV*, pages 2088–2095, 2011. [2](#)
- [35] I. Oikonomidis, Nikolaos Kyriazis, and Antonis A. Argyros. Tracking the articulated motion of two strongly interacting hands. In *CVPR*, pages 1862–1869, 2012. [2](#)
- [36] Paschalis Panteleris, Nikolaos Kyriazis, and Antonis A. Argyros. 3d tracking of human hands in interaction with unknown objects. In *BMVC*, pages 123.1–123.12, September 2015. [2](#)
- [37] P. Panteleris, I. Oikonomidis, and Antonis A. Argyros. Using a single rgb frame for real time 3d hand pose estimation in the wild. *2018 IEEE Winter Conference on Applications of Computer Vision (WACV)*, pages 436–445, 2018. [1](#), [2](#), [3](#)
- [38] Kiru Park, T. Patten, and M. Vincze. Pix2pose: Pixel-wise coordinate regression of objects for 6d pose estimation. In *ICCV*, pages 7667–7676, 2019. [6](#)
- [39] Georgios Pavlakos, Nikos Kolotouros, and Kostas Daniilidis. Texturepose: Supervising human mesh estimation with texture consistency. In *ICCV*, pages 803–812, 2019. [5](#), [7](#)
- [40] Georgios Pavlakos, Luyang Zhu, Xiaowei Zhou, and Kostas Daniilidis. Learning to estimate 3d human pose and shape from a single color image. In *CVPR*, pages 459–468, 2018. [1](#), [5](#), [7](#)
- [41] J. Romero, Dimitrios Tzionas, and Michael J. Black. Embodied hands: Modeling and capturing hands and bodies together. *ACM Transactions on Graphics (TOG)*, 36:1 – 17, 2017. [3](#), [5](#), [7](#)
- [42] Olaf Ronneberger, Philipp Fischer, and Thomas Brox. U-Net: Convolutional Networks for Biomedical Image Segmentation. In *MICCAI 2015*, pages 234–241, 2015. [2](#), [4](#)

- [43] B. Smith, Chenglei Wu, He Wen, Patrick Peluse, Yaser Sheikh, J. Hodgins, and Takaaki Shiratori. Constraining dense hand surface tracking with elasticity. *ACM Transactions on Graphics (TOG)*, 39:1 – 14, 2020. [2](#), [3](#)
- [44] Adrian Spurr, Umar Iqbal, Pavlo Molchanov, Otmar Hilliges, and Jan Kautz. Weakly supervised 3d hand pose estimation via biomechanical constraints. In *ECCV*, pages 211–228, 2020. [1](#)
- [45] Srinath Sridhar, F. Mueller, M. Zollhöfer, D. Casas, Antti Oulasvirta, and C. Theobalt. Real-time joint tracking of a hand manipulating an object from rgb-d input. In *ECCV*, 2016. [2](#)
- [46] O. Taheri, N. Ghorbani, Michael J. Black, and Dimitrios Tzionas. Grab: A dataset of whole-body human grasping of objects. In *ECCV*, 2020. [3](#), [5](#)
- [47] Jonathan Taylor, L. Bordeaux, T. Cashman, Bob Corish, Cem Keskin, T. Sharp, E. Soto, David Sweeney, Julien P. C. Valentin, B. Luff, A. Topalian, E. Wood, S. Khamis, P. Kohli, S. Izadi, R. Banks, A. Fitzgibbon, and J. Shotton. Efficient and precise interactive hand tracking through joint, continuous optimization of pose and correspondences. *ACM Transactions on Graphics (TOG)*, 35:1 – 12, 2016. [2](#)
- [48] Jonathan Taylor, V. Tankovich, Danhang Tang, Cem Keskin, David Kim, Philip L. Davidson, Adarsh Kowdle, and S. Izadi. Articulated distance fields for ultra-fast tracking of hands interacting. *ACM Transactions on Graphics (TOG)*, 36:1 – 12, 2017. [2](#)
- [49] Bugra Tekin, Federica Bogo, and M. Pollefeys. H+o: Unified egocentric recognition of 3d hand-object poses and interactions. *CVPR*, pages 4506–4515, 2019. [1](#), [2](#), [3](#), [6](#)
- [50] H. F. Tung, H. Tung, Ersin Yumer, and K. Fragkiadaki. Self-supervised learning of motion capture. In *NIPS*, 2017. [1](#)
- [51] Dimitrios Tzionas, Luca Ballan, A. Srikantha, Pablo Aponte, M. Pollefeys, and Juergen Gall. Capturing hands in action using discriminative salient points and physics simulation. *International Journal of Computer Vision*, 118:172–193, 2016. [2](#)
- [52] Dimitrios Tzionas and Juergen Gall. 3d object reconstruction from hand-object interactions. In *ICCV*, pages 729–737, 2015. [2](#)
- [53] Ashish Vaswani, Noam Shazeer, Niki Parmar, Jakob Uszkoreit, Llion Jones, Aidan N. Gomez, Lukasz Kaiser, and Illia Polosukhin. Attention is all you need. In *NeurIPS*, pages 5998–6008, 2017. [1](#), [4](#)
- [54] J. Wang, F. Mueller, F. Bernard, Suzanne Sorli, Oleksandr Sotnychenko, Neng Qian, M. Otaduy, D. Casas, and C. Theobalt. Rgb2hands: real-time tracking of 3d hand interactions from monocular rgb video. *ACM Trans. Graph.*, 39:218:1–218:16, 2020. [1](#), [2](#), [3](#)
- [55] Donglai Xiang, Hanbyul Joo, and Yaser Sheikh. Monocular total capture: Posing face, body, and hands in the wild. In *CVPR*, pages 10957–10966, 2019. [2](#)
- [56] Yu Xiang, Tanner Schmidt, Venkatraman Narayanan, and Dieter Fox. Posecnn: A convolutional neural network for 6d object pose estimation in cluttered scenes. *Robotics: Science and Systems XIV (RSS)*, 2018. [3](#), [7](#), [10](#)
- [57] Fuzhi Yang, Huan Yang, J. Fu, Hongtao Lu, and B. Guo. Learning texture transformer network for image super-resolution. In *CVPR*, pages 5790–5799, 2020. [2](#), [3](#)
- [58] Y. Zhou, Connelly Barnes, Jingwan Lu, Jimei Yang, and H. Li. On the continuity of rotation representations in neural networks. In *CVPR*, pages 5738–5746, 2019. [6](#)
- [59] Xizhou Zhu, Weijie Su, Lewei Lu, Bin Li, Xiaogang Wang, and Jifeng Dai. Deformable detr: Deformable transformers for end-to-end object detection. In *ICLR*, 2021. [2](#), [3](#), [4](#)
- [60] C. Zimmermann and T. Brox. Learning to estimate 3d hand pose from single rgb images. In *ICCV*, pages 4913–4921, 2017. [1](#)
- [61] C. Zimmermann, D. Ceylan, Jimei Yang, Bryan C. Russell, Max Argus, and T. Brox. Freihand: A dataset for markerless capture of hand pose and shape from single rgb images. pages 813–822, 2019. [2](#), [3](#)